arXiv:cond-mat/0208117v1 [cond-mat.stat-mech] 6 Aug 2002

Statistical analysis of air and sea temperature anomalies

Nicola Scafetta[1,2], Tim Imholt[2], Paolo Grigolini[2,3,4], and Jim Roberts[2].
[1] *Pratt School EE Dept., Duke University, P.O. Box 90291, Durham, North Carolina 27708*
[2] *Center for Nonlinear Science, University of North Texas, P.O. Box 311427, Denton, Texas 76203-1427*
[3] *Dipartimento di Fisica dell'Università di Pisa and INFM, Piazza Torricelli 2, 56127 Pisa, Italy*
[4] *Istituto di Biofisica CNR, Area della Ricerca di Pisa, Via Alfieri 1, San Cataldo 56010 Ghezzano-Pisa, Italy*
(February 1, 2008)

This paper presents a global air and sea temperature anomalies analysis based upon a combination of the wavelet multiresolution analysis and the scaling analysis methods of a time series. The wavelet multiresolution analysis decomposes the two temperature signals on a *scale-by-scale* basis. The *scale-by-scale* smooth and detail curves are compared and the correlation coefficients between each couple of correspondent sets of data evaluated. The scaling analysis is based upon the study of the spreading and the entropy of the diffusion generated by the temperature signals. Therefore, we jointly adopt two distinct methods: the Diffusion Entropy Analysis (DEA) and the Standard Deviation Analysis (SDA). The joint use of these two methods allows us to establish with more confidence the nature of the signals, as well as their scaling, and it yields the discovery of a slight Lévy component in the two temperature data sets. Finally, the DEA and SDA are used to study the wavelet residuals of the two temperature anomalies. The temporal regions of persistence and antipersistence of the signals are determined and the non-stationary effect of the 10-11 year solar cycle upon the temperature is studied. The temperature monthly data cover the period from 1860 to 2000 A.D.E.

05.45.Tp, 05.45.Df

I. INTRODUCTION

The statistical analysis of time series is a challenging problem of statistical mechanics. This is due to the fact that there are still many unsettled problems. The most important seems to be that the techniques of analysis that are currently used are based on the assumption that the time series under study are generated by stationary processes. In general this is not the case. The time series mirroring complex processes are usually non-stationary in nature. The non-stationary condition seems to be a very general property, although it has any number of possible sources in any system. For instance the origin of non-stationarity in the case of solar flares is given by the solar cycles (for a recent review about this interesting issue, see Ref. [1]) and a special caution must be adopted to take the effects of this non-stationarity into account [2]. In fact, it has been recently shown [3] that the memory left after detrending annual periodicity is much less intense than imagined in earlier publications [4]. Another issue, which seems to be still unsettled, is as to the statistical nature of the fluctuations, once their genuinely stationary nature has been assessed. Are these fluctuations Gaussian? Are these fluctuation of Lévy in nature?

In this paper we want to illustrate an efficient approach to the solution of these difficulties. To stress the efficiency of this approach we apply it to the analysis of global air and sea temperature anomalies, a problem where, as we shall see, properly detrending non-stationary components is an essential request to shed light into the nature of the process under study. The approach we intend to use rests on the joint use of the Diffusion Entropy Analysis (DEA) and wavelet analysis of time series. DEA was born as an efficient way to detect scaling [3,5,6], with applications to sociological [3] and astrophysical [2] processes. This technique of analysis has been applied with success also to the study of DNA sequences [7,8] and heart beat rhythms in cardiac patients [9]. Furthermore, some attention has been devoted to establish the connection between DEA and the Kolmogorov complexity [10] and it is becoming clear that this technique can also be used to study the transition from dynamics to thermodynamics, a crucial property that is used with success to study small portions of large sequences [7], thereby establishing a possible way to address the problem of non-stationality. Research work is currently being done to make it possible to utilize this technique to address the cases of multiple scaling [11].

Wavelet techniques are a powerful method of analysis [12] that localizes a signal simultaneously in time and frequency. We use wavelets for the purpose to decompose the signal in smooth, detail and residual components. The wavelet decomposition has been shown to be an efficient way of detrending from the data a non-stationary component in a natural way, so as to bypass the main difficulties concerning the non-stationary nature of the data under study [13]. The adoption of DEA makes the scaling emerge and also sheds light into the statistical nature of the fluctuations around the non-stationary bias.

Let us now illustrate the time series under study in this paper. The time series of annually averaged global surface temperature anomalies have attracted the attention

of many scientists since the pioneering work of Nicolis and Nicolis [14]. Dynamical systems theory has provided a new quantitative perspective on the predictability of weather and climate processes. For more recent attempts along these lines the interested reader can consult the work of Ref. [15]. The conceptual paradigm behind our analysis is that of intermittence as a dynamic source of Lévy statistics [11]. The detection of Lévy scaling [6] after detrending the non-stationary component would corroborate the validity of an intermittent dynamic model.

It is worth remarking that the term *temperature anomalies* is a technical definition adopted in the current literature on weather and climate processes on earth to denote air and sea temperature departures from a mean temperature value. Therefore, this term must not be confused with the term anomalous diffusion that is related to our conceptual paradigm. We use the data on temperature fluctuations to generate a diffusion process that is compared to the standard Brownian motion. The departure of this resulting diffusion process from Brownian diffusion is called anomalous diffusion. The DEA aims at measuring the strength of this anomaly. Consequently, we can say that one of the aims of this paper is to determine the anomalous nature of the diffusion process generated by air and sea temperature anomalies. The data analyzed are updated continuously by the Climate Research Unit in the United Kingdom [16] and the Hadley Centre for Climate Prediction and Research, Meteorological Office [17]. The earliest of attempts at collecting these data were done in 1986 [18] and has culminated in what is recognized as one of the most accurate data files for global air temperature, and global sea surface temperature (SST) [19]. The land-air temperature has been corrected for non-climatic errors, such as changes in the location of the weather stations and changes in instrumentation [20]. The SST data have been corrected for changes in instrumentation that was used before 1942 [21–23]. The data consists of numbers that represent the departure from a mean temperature in order to see a change from a global average of sorts. The mean temperature used was the 1961-1990 mean temperature.

Figs. 1 show the global air (a) and sea (b) temperature anomalies in the period from 1860 to 2000 A.D.E. The dashed lines are the wavelet multiresolution S7 smooth portion of the signal. The exact mathematical definition of wavelet smooth curve is given in Section 3. To understand the meaning of the data illustrated in Fig. 1, it is enough for the reader to consider the S7 smooth as a convenient way to establish a type of mean value about which the temperature fluctuations take place. In fact, as it will become clear in Section 3, the S7 smooth is obtained by a wavelet average of the data over time intervals of 128 months.

The global air and sea temperature anomalies are very similar to one another. The mean value of temperature fluctuation shows that from 1860 to 1915 the average temperature is almost constant, with a change of only 0.2^o Celsius. From 1915 to 1950 the temperature increases by 0.6^o Celsius. From 1945 to 1980 the average temperature remains almost constant again. Finally, from 1980 to current time there is a further increase of the average temperature of almost 0.4^o Celsius. What about the fluctuations around this mean value? Figs. 2 show the spectral density against the period in months of the global air (a) and sea (b) temperature anomalies in the period from 1860 to 2000 A.D.E.. Some of these periodicities are reported in Table I. The main periodicities involve a time period 6 and 12 months long (related to the yearly cycle of the Earth orbiting the Sun), 9-12 years long, 21-22 years long and, finally, a strong periodicity 55-57 years long (the last three cycles are all established solar cycles with the 9-12 year cycle being the most widely known and observed one).

This paper aims at settling several questions concerning these data. The correlation among air and sea temperature smooth curves seems to be evident. However, it is not so clear if these correlations exist also at the level of fluctuations. Is there anomalous scaling? If there is anomalous scaling, does it rest on smooth curves or fluctuations? Which is the statistical nature of these fluctuations? Are they Gaussian fluctuations? Are they Lévy fluctuations?

The outline of the paper is as follows. In Section 2, to make the paper as self contained as possible, we make a short review of wavelet multiresolution analysis. Section 3 is devoted to the study of the correlation between global air and sea temperature anomalies at the scale of both the wavelet smooth and detail curves. Section 4 is a short review of the DEA and shows this technique at work on the data without any decomposition. Section 5 illustrates the joint use of wavelets and DEA. Finally, in Section 6 we make a balance on the results obtained in this paper.

II. WAVELET MULTIRESOLUTION ANALYSIS

Wavelet analysis [12] is a powerful method to analyze time series that is attracting the attention of an ever increasing number of investigators. Wavelet Transform makes use of scaling functions, the wavelets, which are characterized by the important property of being localized in both time and frequency. These functions integrate to zero and, usually, are normalized. A scaling coefficient τ characterizes a wavelet. The length 2τ measures the width of the wavelet and defines the time scale analyzed by the wavelet. Two typical wavelet functions that are widely used in the continuous wavelet transform are the Haar wavelet and the Mexican hat wavelet [12]. The Haar wavelet is defined as:

$$ {}^{(H)}\tilde{\psi}_{\tau,t}(u) \equiv \begin{cases} -1/\sqrt{2\tau}, & t-\tau < u < t \\ 1/\sqrt{2\tau}, & t < u < t+\tau \\ 0, & otherwise \end{cases} . \quad (1) $$

The Mexican hat wavelet is the second derivative of a Gaussian function. Given a signal $\xi(u)$, the Continuous Wavelet Transform is defined by

$$ W(\tau,t) = \int_{-\infty}^{\infty} \tilde{\psi}_{\tau,t}(u)\ \xi(u)\ du\ . \quad (2) $$

The original signal can be recovered from its Continuous Wavelet Transform via

$$ \xi(u) = \frac{1}{C_{\tilde{\psi}}} \int_0^{\infty} \left[\int_{-\infty}^{\infty} W(\tau,t)\ \tilde{\psi}_{\tau,t}(u)\ dt \right] \frac{d\tau}{\tau^2}\ , \quad (3) $$

where $C_{\tilde{\psi}}$ is a constant that depends on the wavalet function [12]. The double integral of Eq. (3) suggests that the original signal may be decomposed in "continuous details" that depend on the scale coefficient τ. However, there exists a discrete version of the wavelet transform, the Maximum Overlap Discrete Wavelet Transform (MODWT), which is the basic tool needed for studying time series of N data via wavelet. In the Ref. [12], the reader can find all of the mathematical details. For the purpose of this paper, it is important to have in mind only one of the important properties of the MODWT: the Wavelet Multiresolution Analysis (WMA). It is possible to prove that given an integer J_0 such that $2^{J_0} < N$, where N is the number of the data points, the original time series represented by the vector $\mathbf{X}$ can be decomposed as follows:

$$ \mathbf{X} = S_{J_0} + \sum_{j=1}^{J_0} D_j\ , \quad (4) $$

with

$$ S_{j-1} = S_j + D_j\ . \quad (5) $$

The detail D_j represents changes on a scale of $2\tau = 2^j$, while the smooth S_{J_0} represents averages on a scale of $2\tau_{J_0} = 2^{J_0}$. We term wavelet *residuals* the quantities

$$ R_{J_0} = \mathbf{X} - S_{J_0} = \sum_{j=1}^{J_0} D_j\ . \quad (6) $$

It is then evident that we can interpret the residuals as fluctuations about the local mean value evaluated on the time scale $2\tau_{J_0} = 2^{J_0}$. At this stage, the reader should fully understand the comments made in Section 1 about the data illustrated in Fig. 1.

For the reader to properly appreciate the value of WMA, we show this technique at work by means of the results illustrated in Figs. 3 and 4. These figures show the WMA of the global air and sea temperature anomalies in the years 1860-2000. The analysis is done by using the Daubechies *least asymmetric* scaling wavelet filter (LA8) [12]. The LA8 wavelets look similar to the Mexican hat but they are asymmetric, a fact that makes them more plastic than the Mexican hat wavelet. We have plotted the WMA for $J_0 = 7$. Figs. 3 compare the smooth curves S4, S5, S6 and S7 and the detail curves D4, D5, D6, D7 of the air (solid lines) and sea (dashed lines) temperature data. Figs. 4 show the details D1, D2, D3 and D4 of the two sets of data. Details D_j show the fluctuations of the temperature on a scale of $2\tau = 2^j$ months. According to Eqs. (4) and (5), the sum of all seven details and the $S7$ smooth give the two original signals. The $S6$ smooth curve is given by $S7 + D7$; the $S5$ smooth is given by $S6 + D6$, and so on, till to $S1$, given by $S2 + D2$.

Figs. 3 show that the global air and sea temperature anomalies are closely correlated to each other but they do not coincide. If it happens that in a given time region air is hotter than sea, immediately afterward the opposite effect takes place, and sea is warmer than air. The smooth curves of Figs. 3, and especially the S7 and S6 smooth curves, show that in the time regions of persistent temperature increase (time regions 1860-1880, 1910-1950 and 1980-2000) air is hotter. Instead, in the time regions of persistent temperature decrease (time regions 1880-1910 and 1950-1980) air is colder. This may be explained by the fact that heat capacity of water is higher than heat capacity of air, thereby implying that it takes more time for water temperature either to increase or to decrease. The D4, D5, D6, D7 details illustrate the temperature fluctuations of both air and sea corresponding to the time scales of 16, 32, 64 and 128 months respectively. The fluctuations of both kinds of data, air and sea, look remarkably similar. The analysis of the details D1, D2 and D3 of Figs. 4 show, instead, that the fluctuations of the air temperature are larger than those of the sea temperature. This effect, too, may be related to the higher heat capacity of water. Finally, Figs. 4 show a stronger fluctuation of the data during the period 1860-1880. There is also a strong fluctuation of sea temperature in the D3 detail, in the 1920-1950 time region. Further study is required to assess whether these stronger fluctuations are due to natural phenomena or to some artifact of a non conventional way of data acquisition.

III. MULTIRESOLUTION CORRELATION ANALYSIS

The use of the Multiresolution Correlation Analysis via wavelet is a simple procedure [24]. We decompose the two temperature datasets into rests and details by using WMA as demonstrated in the previous section. Then,

we create pairs of partners, the first component of the pair being either a rest or a detail of the sea temperature data and the second the corresponding rest or detail of the air temperature data. For any given pair of datasets (x_i, y_i); $i = 1, ..., N$, the linear correlation coefficient r is given by the formula

$$r = \frac{\sum_i (x_i - \overline{x})(y_i - \overline{y})}{\sqrt{\sum_i (x_i - \overline{x})^2}\sqrt{\sum_i (y_i - \overline{y})^2}} , \qquad (7)$$

where, as usual, $\overline{x}$ is the mean of the former sequence and, $\overline{y}$ is the mean of the latter sequence. The value of r lies between -1 and 1, and can include the extreme values 1 and -1. It takes on a value of 1, termed "completely positive correlation," when the data points lie on a perfect straight line with positive slope, with x and y increasing together. The value 1 holds independently of the magnitude of the slope. If the data points lie on a perfect straight line with negative slope, y decreasing as x increases, then r has the value -1; this is called "completely negative correlation." A value of r near zero indicates that the variables x and y are uncorrelated. The two sequences are considered to be significantly correlated when the value of $|r|$ is close to 1.

Fig. 5 illustrates the correlation coefficient, r, between air and sea temperature anomalies as a function of the wavelet index j, and thus, for the reasons illustrated in Section 3, as a function of the wavelet scale $2\tau = 2^j$. The top curve denotes the correlation between the air and the sea S_j smooth curves, with j ranging from 0 to 10. The bottom curve denotes the coefficient of correlation between air and sea details, D_j, with j ranging from 1 to 10. The value $r = 0.87$ corresponding to the top curve at $j = 0$ is the correlation coefficient between the two original temperature data without any filtering. For the sake of reader's convenience the values of r are reported in Table II. From Fig. 5 we see the small details D1, D2, D3 and D4 are not significantly correlated. These details refer to a time scale until 16 months, and consequently we can conclude that within this time range there are no significant correlations between sea and temperature fluctuations. The correlation between the details increases with increasing the scale index and becomes significant for D5, D6 and D7. The reader can consult Figs. 3, which confirms in fact visually that these details are significantly correlated. The correlation between the D7 details yields a local maximum, $r = 0.95$. All this means that the S4-S7 smooth curves are the best indicators of the correlations between air and sea temperature anomalies. In fact, according to the prescriptions of Section 3, the S4-S7 smooth curves are obtained by adding to S4 the D5, D6 and D7 details, respectively, and these details, as shown by the bottom curve of Fig. 5 are correlated. Again, the reader can make a visual inspection of these smooth curves by consulting Figs 3. Details smaller than the D5 detail have small correlations. This also means that to shed light on the properties that make sea temperatures different from air temperatures we must focus on small details. Smooth curves larger than S7 are very well correlated but do not afford additional information, because they are too smooth.

IV. SCALING ANALYSIS

Scale invariance has been found to hold empirically for a number of complex systems [25] and the correct evaluation of the scaling exponents is of fundamental importance to assess if universality classes exist [26]. A widely used method of analysis of complexity rests on the assessment of the scaling exponent of the diffusion process generated by a time series. See, for instance, Refs. [3,5,7,8,27]. According to the prescription of Ref. [27], we interpret the numbers of a time series as generating diffusion fluctuations and we shift our attention from the time series to the probability distribution function (pdf) $p(x, t)$, where x denotes the variable collecting the fluctuations. The scaling property takes on the form

$$p(x, t) = \frac{1}{t^\delta} F\left(\frac{x}{t^\delta}\right) , \qquad (8)$$

where δ is the scaling exponent.

A. Gauss and Lévy diffusion

There are two main forms of anomalous diffusion. The first is the generalization of Brownian motion, proposed years ago by Mandelbrot [25], known as Fractional Brownian Motion (FBM) and yielding for the diffusion process a variance increasing in time as t^{2H}. This kind of anomalous diffusion fits the scaling definition of Eq.(8) with $\delta = H$ and $F(y)$ being a Gaussian function of y. A second form of anomalous diffusion is obtained by generalizing the Central Limit Theorem (CLT). The prescriptions of the Generalized Central Limit Theorem (GCLT) [28] are as follows. Let us assume that the diffusing variable x is the sum of t independent random variables ξ_i, each of which has a probability distribution, symmetric around $\xi = 0$. Let us assume also that for large values of $|\xi|$, this distribution is an inverse power law, with index $\mu > 1$, so as to fit the normalization condition, and $\mu < 2$, so as to violate the CLT constraint. Then, according to the GCLT, for $t \to \infty$, the diffusion becomes stable and the Fourier transform of $p(x, t)$ gets the form

$$\hat{p}(k, t) = \exp\left(-b|k|^\alpha t\right) , \qquad (9)$$

where b is a kind of generalized diffusion coefficient, determined by the strength of the fluctuations and $\alpha = \mu + 1$. It has been shown [28] that there is scaling. This

means that the resulting diffusion process fits the condition of Eq. (8), with $\delta = 1/\alpha$, namely,

$$\mu = 1 + \frac{1}{\delta}. \tag{10}$$

Both forms of anomalous diffusion are idealization of reality. The theory of FBM implies that the corresponding scaling property holds true at any time scale, while its dynamic derivation [29], in the persistent case $H > 0.5$, suggests that it is a time asymptotic property generated by the fluctuations of a Gaussian variable $\xi(t)$, whose correlation function has inverse power law with index $\beta < 1$ ($H = 1 - \beta/2$). The main problem with this dynamic interpretation is that there are no stable theorems behind the Gaussian property of the "microscopic" fluctuation $\xi(t)$. It is necessary to supplement the dynamic model with random ingredients that do not have a dynamic origin [30]. The earlier illustrated approach to Lévy statistics, called Lévy flight, is judged to be unrealistic, because it involves a random velocity that can be arbitrarily large. To bypass this difficulty recourse is given to Lévy walk [31]. We adopt the following dynamic model [11]. Let us consider a sequence $\{\tau_i, s_j\}$, with $i = 0, 1, ..., \infty$. The numbers τ_i are random numbers with the distribution density

$$\psi(\tau) = (\mu - 1)\frac{T^{\mu-1}}{(T+\tau)^{\mu}} \ , \tag{11}$$

where T is a positive constant. Note that to ensure the stationary condition the additional condition $\mu > 2$ is necessary, and we make this assumption also in this paper. Thus, we have $\mu < 3$ to ensure the anomalous character of the resulting diffusion process and $\mu > 2$ to make our dynamic picture stationary. It is easy to prove that $< \tau >= T/(\mu - 2)$. The numbers s_i have the values 1 and -1, determined by the coin tossing rule. For a generic time t, let us consider the time t_N fitting the conditions $t_N = \tau_0 + \tau_1 + ...\tau_{N-1} + \tau_N < t$ and $t_N + \tau_N > t$. Then the trajectory prescribed by this dynamic model is $x(t) = W[\tau_0 s_0 + \tau_1 s_1 + ...\tau_{N-1} s_{N-1} + (t - t_N)s_N]$. We see that in this case, due to the large memory time, the random walkers can travel ahead or backwards by quantities with the same distribution as the Lévy flight. However, this takes a time proportional to the traveled length. The correlation functions of each elementary jumps, either W or $-W$ has an inverse power law with index β, which is now given by $\beta = \mu - 2$. It is important to notice that the process is now multiscaling [11], due to the fact that the propagation fronts propagate linearly in time. The central part of the distribution, if we neglect the truncation produced by the finite velocity of the propagation front, is given by $\delta = 1/(\mu - 1)$, namely, by Eq.(10).

It is important to stress that this dynamic model to Lévy statistics yields, at any finite time t, finite second moments. Consequently, it could be interpreted as a form of FBM. However, in this case H would not correspond to the correct scaling of the central part of the distribution and δ and μ are related to this pseudo-scaling H by [6].

$$\delta = \frac{1}{3 - 2H} \ . \tag{12}$$

and

$$\mu = 4 - 2H, \tag{13}$$

respectively.

B. The diffusion algorithm

Let us consider a sequence of N numbers

$$\xi_i, \quad i = 1, \ldots, N. \tag{14}$$

The goal is to establish the possible existence of a scaling, either normal or anomalous, in the most efficient way as possible without altering the data with any form of detrending. First of all, let us select an integer number t, fitting the condition $1 \leq t < N$. This integer number will be referred to by us as "diffusion time". For any given time t we can find $M(t) = N - t + 1$ sub-sequences defined by

$$\xi_i^{(s)} \equiv \xi_{i+s}, \quad with \quad s = 0, \ldots, N - t. \tag{15}$$

For any of these sub-sequences we build up a diffusion trajectory, s, defined by the position

$$x^{(s)}(t) = \sum_{i=1}^{t} \xi_i^{(s)} = \sum_{i=1}^{t} \xi_{i+s}. \tag{16}$$

The direct evaluation of variance is probably the most natural method of variance detection. All trajectories start from the origin $x(t = 0) = 0$. With increasing time t, the sub-sequences generate a diffusion process. At each time t, it is possible to calculate the Standard Deviation of the position of the $M(t)$ sub-sequences with the well known expression:

$$D(t) = \sqrt{\frac{\sum_{s=0}^{N-l} \left[x^{(s)}(t) - \overline{x}(t)\right]^2}{M(t) - 1}}, \tag{17}$$

where $\overline{x}(t)$ is the average of the positions of the $M(t)$ sub-trajectories at time t. The exponent H is defined by

$$D(t) \propto t^H \ . \tag{18}$$

We call this approach to the scaling evaluation Standard Deviation Analysis (SDA). In Ref. [6] the interested reader can find an illustration of the traditional techniques of scaling detection and of why all of them are virtually equivalent to the SDA.

The DEA, is based upon the following algorithm. We have to partition the x-axis into cells of size $\epsilon(t)$. When this partition is made, we have to label the cells. We count how many particles are found in the same cell at a given time t. We denote this number by $N_i(t)$. Then we use this number to determine the probability that a particle can be found in the i-th cell at time t, $p_i(t)$, by means of

$$p_i(t) \equiv \frac{N_i(t)}{M(t)}. \tag{19}$$

At this stage the entropy of the diffusion process at the time t is determined and reads

$$S(t) = -\sum_i p_i(t)\ \ln[p_i(t)]\ . \tag{20}$$

The easiest way to proceed with the choice of the cell size, $\epsilon(t)$, is to assume it to be a fraction of the square root of the variance of the fluctuations $\xi(i)$, and consequently independent of t. If the scaling condition of Eq. (8) holds true, it is easy to prove that

$$S(t) = A + \delta\ \ln(t)\ , \tag{21}$$

where, in the continuous approximation,

$$A \equiv -\int_{-\infty}^{\infty} dy\, F(y)\ \ln[F(y)]\ , \tag{22}$$

with $y = x/t^{\delta}$. The scaling Eqs. (18) and (21) determine the exponents H and δ.

C. Data analysis

Fig. 6 shows the numerical results by using the DEA (Figs. 6a and 6c) and the SDA (Figs. 6b and 6d) of the global air (Figs. 6a and 6b) and sea (Figs. 6c and 6d) temperature anomalies. In the ordinate axis we plot $D(t)/D(1)$ and $S(t) - S(1)$. Thus, the curves start from 1 and 0, respectively. The straight lines are function of the type $f_{DE}(t) = \delta\ \ln(t)$ and $f_{SD}(t) = t^H$ and become straight lines as a consequence of the linear-log (DEA case) and log-log (SDA case) representations we are adopting. The global air temperature anomalies are characterized by a pdf scaling coefficient $\delta_a = 0.87 \pm 0.02$ and a standard deviation scaling coefficient $H_a = 0.92 \pm 0.01$. The global sea temperature anomalies are characterized by a pdf scaling coefficient $\delta_s = 0.89 \pm 0.02$ and a standard deviation scaling coefficient $H_s = 0.94 \pm 0.01$. The figures are plotted for a period $t = 50$ months. For value of t larger than 50, saturation effects due to the statistical property appear. The fitting is a kind of mean result obtained by averaging the results corresponding to fitting the first 20, 30 and 40 points. The upper time limit condition of $t = 50$ is dictated by the fact that we are using N = 1680 data, a number with a square root of about 40. The pictures show that for $t = 50$ the standard deviation is almost 40 times larger than the standard deviation at the first step of diffusion. It seems, therefore, that the statistics are rich enough to get a satisfactory pdf and consequently reliable scaling properties.

The high values of the exponents imply a strong persistence. This means that the temperature changes gradually month by month. The fact that the exponents stemming from the sea temperature anomalies are higher than those produced by the air temperature anomalies means that the sea temperature anomalies are characterized by a persistence higher than that of the air temperature anomalies. This can be explained as an effect of the higher heat capacity of the water. These results confirm the results of Sec. 3, shown in Figs. 4, where the fluctuations of the air temperature anomalies at short scale are stronger than those of the sea temperature anomalies. Finally, we note that the both exponents H_a, for air, and H_s, for sea, are larger than δ_a and δ_s respectively. This means that the pdf of the two diffusion processes is a little bit larger than a Gaussian distribution. The four exponents fulfill the Lévy Walk Diffusion relation (12) within the accuracy of our statistical analysis. This means that global air and sea temperature anomalies not only are characterized by Lévy statistics, but are a manifestation of the dynamic model illustrated in Section 4 A. This means that the alternated periods τ_i of high and low temperature are distributed according an inverse power law with $\mu < 3$. According to Eqs. (13) and (10), we obtain $\mu_a = 2.13 \pm 0.02$ and $\mu_s = 2.08 \pm 0.02$. The results are summarized in Table III.

V. WAVELET MULTIRESOLUTION DIFFUSION ANALYSIS

In this section we introduce a method of analysis, based on the joint use of wavelet decomposition and the diffusion approach to scaling, the latter method resting on both DEA and SDA. This method turns out to be powerful, and we refer to it as Wavelet Multiresolution Diffusion Analysis, WMDA. Figs. 7 and 8 show the SDA and the DEA of the global air (a) and sea (b) temperature applied to the residuals R_j, where, as in the earlier sections, j indicates the wavelet scale index. Each residual contains all details at smaller scales. Therefore, the WMDA allows us to determine the diffusion spreading at each time scale, as stemming from the corresponding details, an important piece of information. The residuals R_j are obtained by detrending the original data with the smooth curves S_j obtained with the wavelet multiresolution analysis; see Eq. (6). In each of the four figures there are nine curves. The figures (a) refer to air, the figures (b) refer to sea. Figs. 7 refer to SDA and Figs. 8 to DEA. From top to bottom the curves of these figures

denote the original data (1), and the residuals (2) R9 (2) , (3) R8 (3) ,..., (9) R2(9) . The curves of Figs. 7 and 8 are an illustration of WMDA and prove that this is a useful tool to study complexity of a dynamical system. Let us analyze them in detail.

a- Figs. 7 and 8 look similar but are not identical. The curves afforded by DEA are more detailed than those obtained by using SDA. This is because DEA is more sensitive to fluctuations than standard deviation, which only measures the spreading of the diffusion trajectories.

b- The straight lines correspond to the function $f_{SD}(t) = t^{0.5}$, in Figs. 7, and to the function $f_{DE}(t) = 0.5\ln(t)$, in Figs. 8, and look straight due to the adoption of the log-log (Figs. 7) and linear-log (Figs. 8) representations. These straight lines serve the purpose of signaling what would be the behavior of an ordinary Gaussian diffusion. According to the Mandelbrot interpretation [25], the curve with slopes larger than that of these straight lines indicate persistent diffusion or superdiffusion, and the curves with slopes smaller than that of these straight lines indicate antipersistent diffusion or a subdiffusion region. By comparing the curves of Figs. 7, resting on SDA, to the corresponding curves of Figs. 8, resting on DEA, we see that the times at which the SDA curves cross the line $f_{SD}(t) = t^{0.5}$ are larger than the times at which the DEA curves cross the line $f_{DE}(t) = 0.5\ln(t)$. This is a further proof that the dynamics behind the data cannot be Fractional Brownian Motion. This kind of diffusion process would imply SDA and DEA crossing the lines denoting ordinary diffusion at the same time. The figures suggest that the diffusion is characterized by a pdf whose tails are more persistent than the Gaussian tails of Fractional Brownian Motion. The analysis of Section 5C proved that the diffusion is anomalous and fulfills the Lévy Walk condition. In this section, with the help of WMDA we show that the data are characterized by an anomalous dynamics at short as well as long time scales.

c- By comparing the curves of Figs. 7a and 8a to the corresponding curves of Figs. 7b and 8b, we note the air temperature curves always have a slope smaller, even if slightly smaller, than the slope of the corresponding sea temperature curves. This means that at each wavelet scale the higher heat capacity of the water makes the sea temperature data more persistent than the air ones. This is related to the higher heat capacity of the water.

d- Figs. 7 and 8 show that each curve is characterized by one leading periodicity. The dynamical reasons for this property are easily accounted for by noticing that a given periodicity of the data causes a periodic convergence of distinct trajectories. After an initial spreading, with a consequent increase of both variance and entropy, there are incomplete regressions of the initial condition. Since each curve corresponds to a given scale, the observed processes of regression correspond to the leading periodicity of that temporal scale. Any residuals R_j contains all details at smaller scales, and, as a consequence, the leading periodicity is not necessarily related to the wavelet temporal scale τ_j by simple relations. For example, the R7 and R8 curves of Figs. 7a and 8a show almost the same periodicity but τ_7 is one half of τ_8. Moreover, the main periodicities do not coincide exactly for the global air and sea temperature anomalies. The figures show that the year periodicity and its multiples have a strong effect until the residual R6. A periodicity of 17-20 years dominates the R7 and R8 residuals. Finally, a periodicity of 57-59 years characterizes the R9 rest. Figs. 7 and 8 show that WMDA may be an interesting complement to the spectral density analysis of Figs. 2 because it shows the main periodicity and its contribution to the information that characterizes that scale level.

e- Figs. 7 and 8 show that both entropy and standard deviation of any residual converges to a horizontal line. This is due to the detrending of the smooth part of the data, S_j, which makes the hidden periodicities show up. At the same time, these hidden periodicities imply the deterministic nature of the signal and consequently yield entropy saturation. In other words, the fluctuations ξ_i of the residuals data R_j can generate trajectories with only a limited spreading. The height of the horizontal lines measures the maximum spreading (in the case of SDA, Figs. 7) and the information or entropy (in the case of DEA, Figs. 8) for each time scale. It is interesting to notice that the shorter the time scale the faster the transition to saturation. This means that the role of periodicities becomes more and more important as we decrease the time scale.

Table IV summarizes some of the information contained in Figs. 7 and 8, and can help the reader to understand the balance of the results of this paper that will be given in Sec. 6.

Finally, the reader may wonder what happens if we detrend one of the wavelet details from the original data. In our analysis we observe that the scaling properties coincide, within the limit of the analysis statistical accuracy, with those of Section 4 C for $t < 50$. This applies to detrending from the original data any detail between D1 and D10. This means that the wavelet smooth curves S determine the scaling because they determine the persistent properties of the signal. The scaling for $t < 50$ is not conditioned by any cycle in the data. If we consider interval larger than $t = 50$ we observe the largest discrepancy by detrending the detail D7. Figs 9a (air) and 9b (sea) show the results. The detrended data have a lower entropy for $30 < t < 200$. This entropy seems to scale with δ close to 0.5 until $t = 600$, like a Brownian diffusion. However, the lack of sufficiently rich statistics in that region does not allow us to get any conclusion about the real value of the scaling. The SDA, instead, does not detect this difference, Figs 9c and 9d; the entropic analysis turns out to be more sensitive than the variance analysis. The increasing of entropy of the original data for $30 < t < 200$ have a non-stationary origin

due to a cycle that is detrended by the detail D7. In fact, detail D7 corresponds to the wavelet time scale of 128 months, that is, 10-11 years, and it contains the important 10-11 years solar cycle.

VI. CONCLUSION

The key results of these paper can be summarized as follows:

(i) *Understanding the various aspects of a global climate system.* Global climate is a complex system in which many factors affect one another and without a detailed look into the behavior of the Earth different temperature systems and their correlations, any attempt to understand it will be difficult at best. For example, understanding these behaviors is important to comprehend local and global climate changes, as well as, to attempt to rebuild past climate more accurately [33]. In fact, our analysis shows that the differences between the behavior of the data on the shorter time scale lends itself to caution when performing these reconstructions. The understanding and reconstruction of climate to times previous to instrumental records will allow us to gain some knowledge of the long term behavior of future climate [34]. We show, in fact, that no significant correlation exists for detail up to time intervals of 16 months. For larger time intervals this correlation becomes visible. Our analysis has shown the differences in the fundamental types of statistical behavior of both regions of the Earth. This knowledge could be used to further our ability to reconstruct past climate in an attempt to better understand our dynamic global environment.

(ii) *Scaling and its relevance for the air and sea temperature anomalies.* The joint use of DEA and SDA allowed us to establish better the nature of the signals, as well as their scaling. The data seems to have a slight Lévy component. The higher scaling of sea signal is interpreted as a consequence of the higher thermal capacity of sea water.

(iii) *Periodicity effects on scaling.* We proved that scaling detected by using the DEA is not affected by periodicities. The smooth curves are responsible for scaling and scaling is not influenced by cycles. The smooth curves are responsible for a steady increase of entropy of the diffusion.

(iv) *Residuals and periodicities.* We showed that periodicities emerge at the level of residuals, namely the portions of the signals obtained detrending the smooth parts. The diffusion entropy of residuals saturates, thereby implying that after a given time there is no further information increase. We can therefore, conclude that there should be no concern about a possible influence of periodicities on scaling. The scaling found is a genuine property and we can freely adopt it as an indicator of correlations. The sea temperature data, yielding a higher scaling, imply a larger correlation and the statistical analysis of this paper makes compelling this important conclusion.

(v) *Details and non-stationary effect.* We show that detail D7, that contains the important 10-11 year solar cycle, causes a non-stationary effect that is detected by DEA but not by SDA. This shows that DEA has a higher sensitivity.

(vi) *Joint use of entropy and decomposition.* We think the benefit of the joint use of DEA and wavelets is evident. The wavelet decomposition generates a set of new time series, corresponding to tuning the wavelet microscope to a given time scale, and the DEA establishes the information of these components, and makes it evident why periodicities set an upper limit on entropy increase.

It is interesting to point out that the earlier analysis of temperature anomalies [14,15] has been done using deterministic chaos and the evaluation of the Lyapunov coefficient, and so the Kolmogorov-Sinai (KS) entropy. Our research work seems to support the dynamical model of Ref. [11] , which is a form of Lévy walk. This means a connection with turbulence and intermittence. The values of μ emerging from this analysis are very close to $\mu = 2$ and thus to the border with the non-stationary dominion [35]. It is known that the KS entropy vanishes for $\mu \leq 2$. The authors of Ref. [15] seem to rest on a condition of vanishing KS entropy to address the intriguing problem of climate predictability. We think therefore that the joint use of DEA and Compression algorithms [10], applied after the wise detrending method illustrated in this paper, might contribute further processes towards the ambitious goal of predictability.

Acknowledgment:

P.G. gratefully acknowledges the financial support received from the Army Research Office through Grant DAAD 19-02-0037 and N.S. thanks the Army Research Office for support under grant DAAG5598D0002.

[1] G. Rudiger and R. Arlt, arXiv:astro-ph/0201129.

[2] P. Grigolini, D. Leddon, N. Scafetta, Phys. Rev. E **65**, 046203 (2002).

[3] N. Scafetta, P. Hamilton and P. Grigolini, Fractals, **9**, 193 (2001).

[4] B.J. West, P. Hamilton and D.J. West, Fractals **7**, 113 (1999).

[5] P. Grigolini, L. Palatella, G. Raffaelli, Fractals, **9**, 439 (2001).

[6] N. Scafetta, P. Grigolini, cond-mat/0202008, in press on PRE.

[7] P. Allegrini, P. Grigolini,, P. Hamilton, L. Palatella, G. Raffaelli and M. Virgilio, *Emergent Nature*, M. M. Novak

(ed.), World Scientific, p. 173 (2002).
[8] N. Scafetta, V. Latora, P. Grigolini, Phys. Lett. A **299**, 565 (2002).
[9] P. Allegrini, P. Grigolini, P. Hamilton, L. Palatella, and G. Raffaelli, Phys. Rev. **65**, 041926-1-5 (2002).
[10] P. Allegrini, V. Benci, P. Grigolini, P. Hamilton, M. Ignaccolo, G. Menconi, L. Palatella, G. Raffaelli, N. Scafetta, M. Virgilio, J. Yang, Chaos, Solitons & Fractals, in press (2002).
[11] P. Allegrini, J. Bellazzini, G. Bramanti, M. Ignaccolo, P. Grigolini, and J. Yang, Phys. Rev. E **66**, 015101 (R) (2002).
[12] D. B. Percival and A. T. Walden, *Wavelet Methods for Time Series Analysis*, Cambrige University Press, Cambrige (2000).
[13] N. Scafetta, P. Grigolini, P. Hamilton and B.J. West, cond-mat/0207536, submitted to PRE.
[14] C. Nicolis, G. Nicolis, Nature **311**, 529 (1984).
[15] L. Gimeno, R. García, J.M. Pacheco, E. Hernández, P. Ribera, Earth Planet. Sci Lett. **184**, 561 (2001).
[16] Climate Research Unit, School of Environmental Sciences, University of East Anglia, Norwich NR4 7TJ, United Kingdom.
[17] Hadley Centre for Climate Prediction and Research, Meteorological Office, Bracknell, Berkshire, United Kingdom.
[18] P.D. Jones, T.L. Wigley, and P.B. Wright. Global temperature variations between 1861 and 1984, *Nature*, 322:430-434, 1986.
[19] P.D. Jones, D.E. Parker, T.J. Osborn, and K.R. Briffa 2001. Global and hemispheric temperature anomaliesland and marine instrumental records. In Trends: A Compendium of data on Global Change. Carbon Dioxide Information Analysis Center, Oak Ridge National Laboratory, U.S. Department of Energy, Oak Ridge, Tenn., U.S.A, 2001.
[20] P.D. Jones, Hemispheric surface air temperature variations: A reanalysis and an update to 1993, *Journal of Climate* 7(11):1794-1802, 1993.
[21] D.E. Parker, P.D. Jones, A. Bevan, and C.K. Folland, Interdecadal changes of surface temperature since the 19th century, *Journal of Geophysical Research* 99:14373-14399, 1994.
[22] D.E. Parker, C.K. Folland, and M. Jackson, Marine surface temperature: observed variations and data requirements, *Climate Change* 31:559-600, 1995.
[23] C.K. Folland, and D.E. Parker, Correction of intrumental biases in historical sea surface temperature data, *Quarterly Journal of the Royal Meteorological Society 121:319-367.*
[24] N. Scafetta, T. Imholt, P. Grigolini, J. Roberts, (submitted to International Journal of Climatology).
[25] B.B. Mandelbrot, *The Fractal Geometry of Nature*, Freeman, New York, 1983.
[26] H.E. Stanley, L.A.N. Amaral, P. Gopikrishnan, P. Ch. Ivanov, T.H. Keitt, V. Plerou, Physica A **281** 60 (2000).
[27] C.-K. Peng, S.V. Buldyrev, S. Havlin, M. Simons, H.E. Stanley, and A.L. Goldberger, Phys. Rev, E **49**, 1685 (1994).
[28] B.V. Gnedenko and A.N. Kolomogorov, *Limit Distributions for Sums of Random Variables*, Addison-Wesley, Reading, MA, 1954.
[29] G. Tréfan, E. Floriani, B. J. West and P. Grigolini, Phys. Rev. E **50** , 2564 (1994).
[30] P. Allegrini, M. Buiatti, P. Grigolini and B. J. West, Phys. Rev. E **57**, 4558 (1998).
[31] J. Klafter, M.F. Shlesinger, and G. Zumofen, Phys. Today **49**(2), 33 (1996); G. Zuomofen, J. Klafter, and M.F. Shlesinger, Lect. Notes Phys **519**,15 (1998).
[32] P. Allegrini, R. Baiocchi, S. Chillemi, P. Grigolini, L. Palatella, G. Raffaelli, in press on Lecture Notes in Computer Science.
[33] M.E. Mann, R.S. Bradley, and M.K. Hughes, Northern Hemisphere Temperatures During the Past Millennium: Inferences, Uncertainties, and Limitations, *Geo. Res. Lett.*, 26, 6, 759-762, 1999.
[34] P.D. Jones, K.R. Briffa, T.P. Barnett, and S.B. Tett, High-resolution paleoclimate records for the last millenium: interpretation, integration and comparison with General Circulation Model control-run temperatures, *The Holocene*, 8,4,455-571, 1998.
[35] M. Ignaccolo, P. Grigolini, A. Rosa, Phys. Rev. E **64**, 026210 (2001).

Figure 1

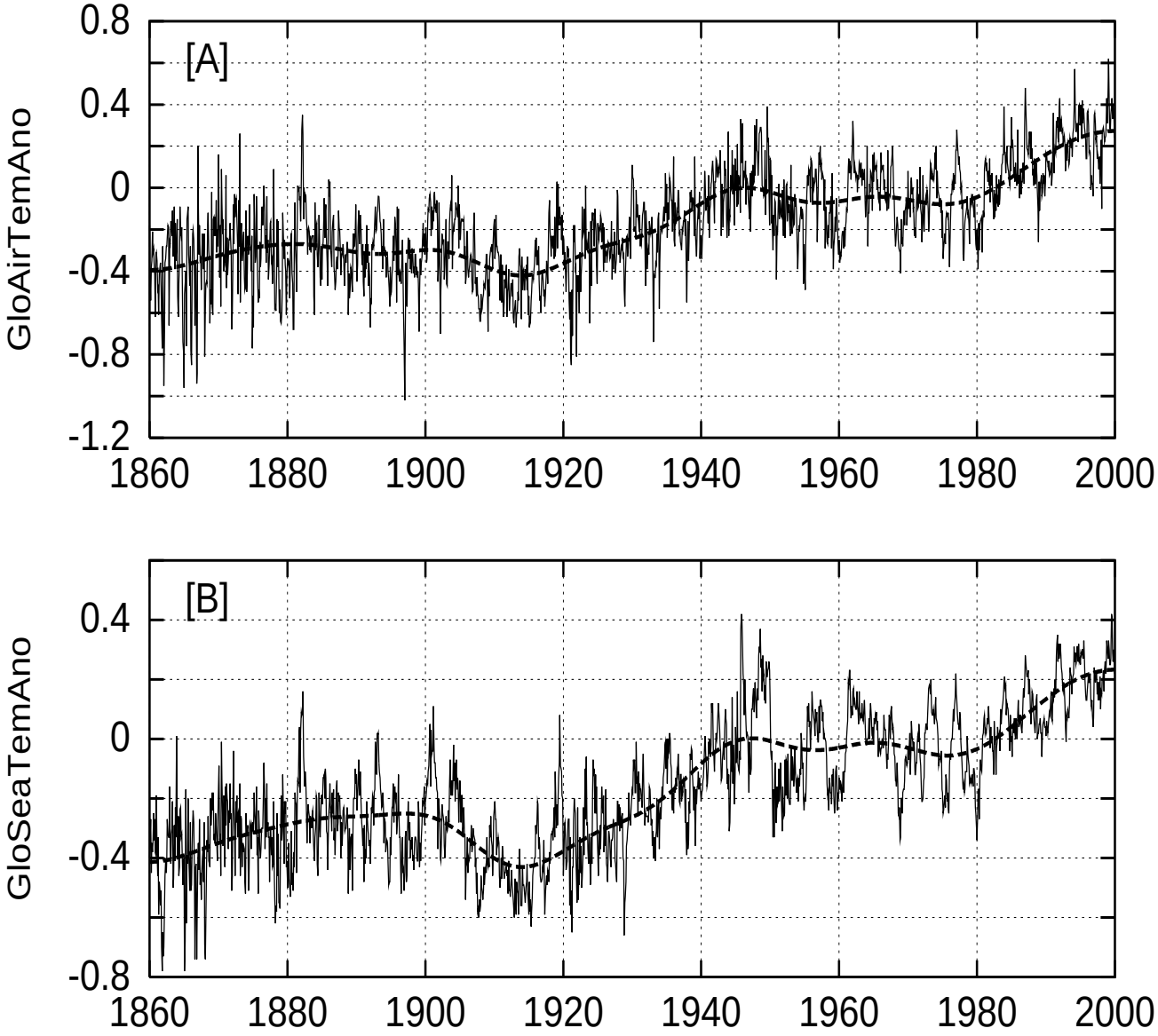

FIG. 1. Global air and sea temperature anomalies in Celsius degree (years: 1860-2000). The dashed lines are the wavelet multiresolution smooth curves S7.

Figure 2

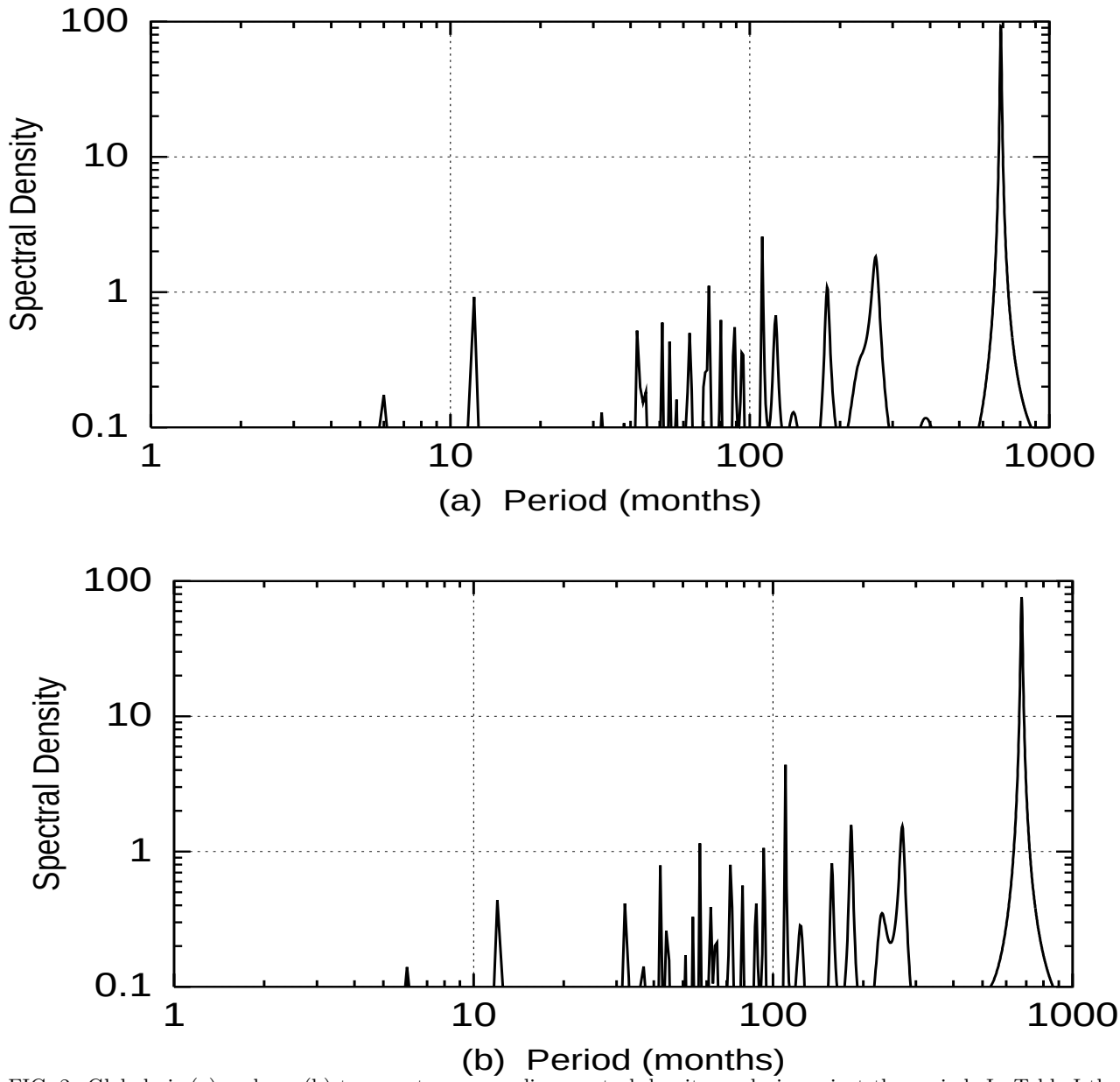

FIG. 2. Global air (a) and sea (b) temperature anomalies spectral density analysis against the period. In Table I there are some of the main periods.

Air	1		3.5	4.25	6.1		9.2	10.2	15.1	21.9	55.7
Sea	1	2.7	3.5	4.75	6	7.75	9.2	12.7	15.2	22.5	56.3

TABLE I. Main periods present in the global air and sea temperature anomalies. The values are in years.

Figure 3

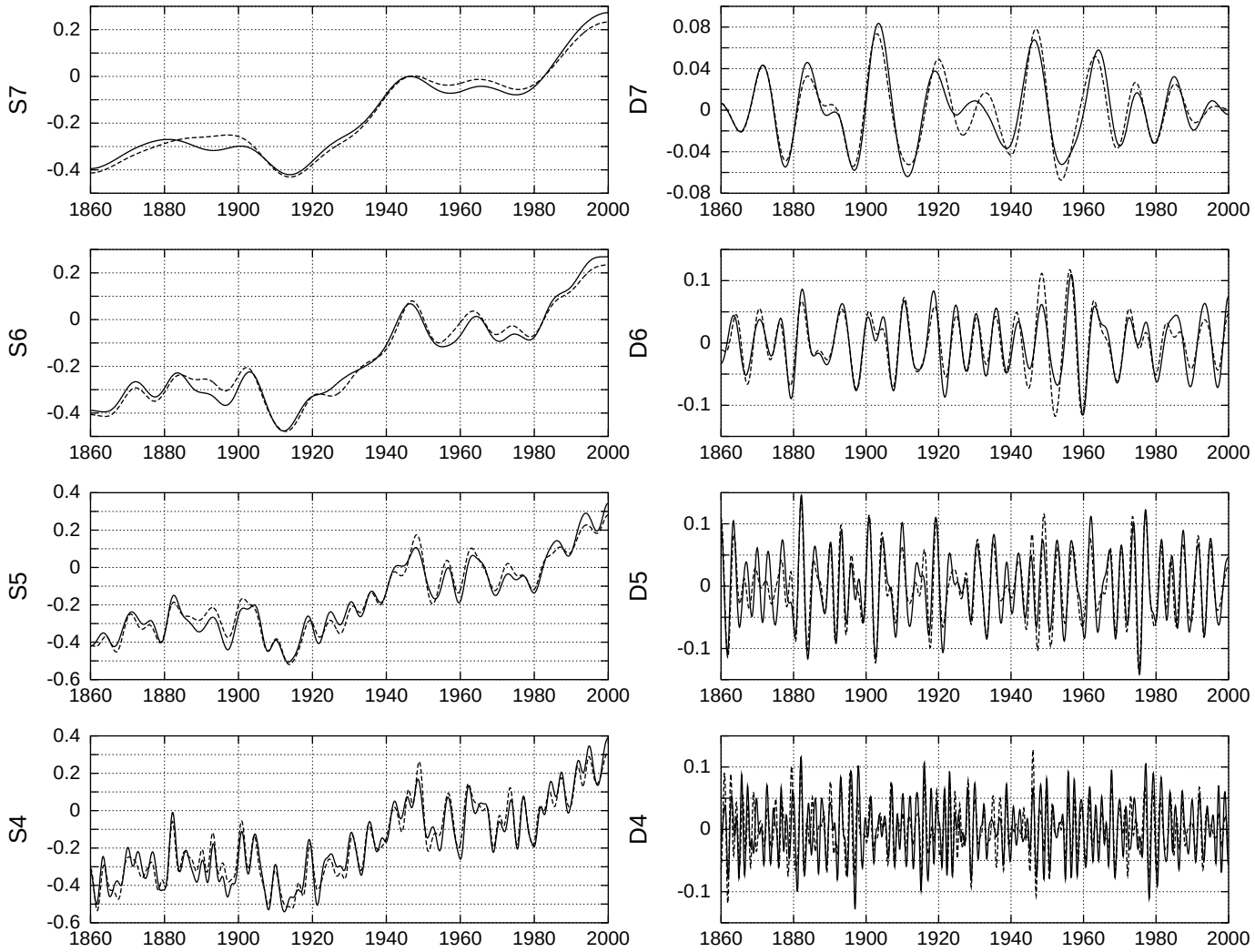

FIG. 3. Wavelet Multiresolution Analysis of the global air (solid lines) and sea (dashed lines) temperature anomalies in Celsius degree. The figures show the smooth curves S7, S6, S5, S4 and the details curves D7, D6, D5 and D4 that are associated to the scales of 256, 128, 64 and 32 months.

Figure 4

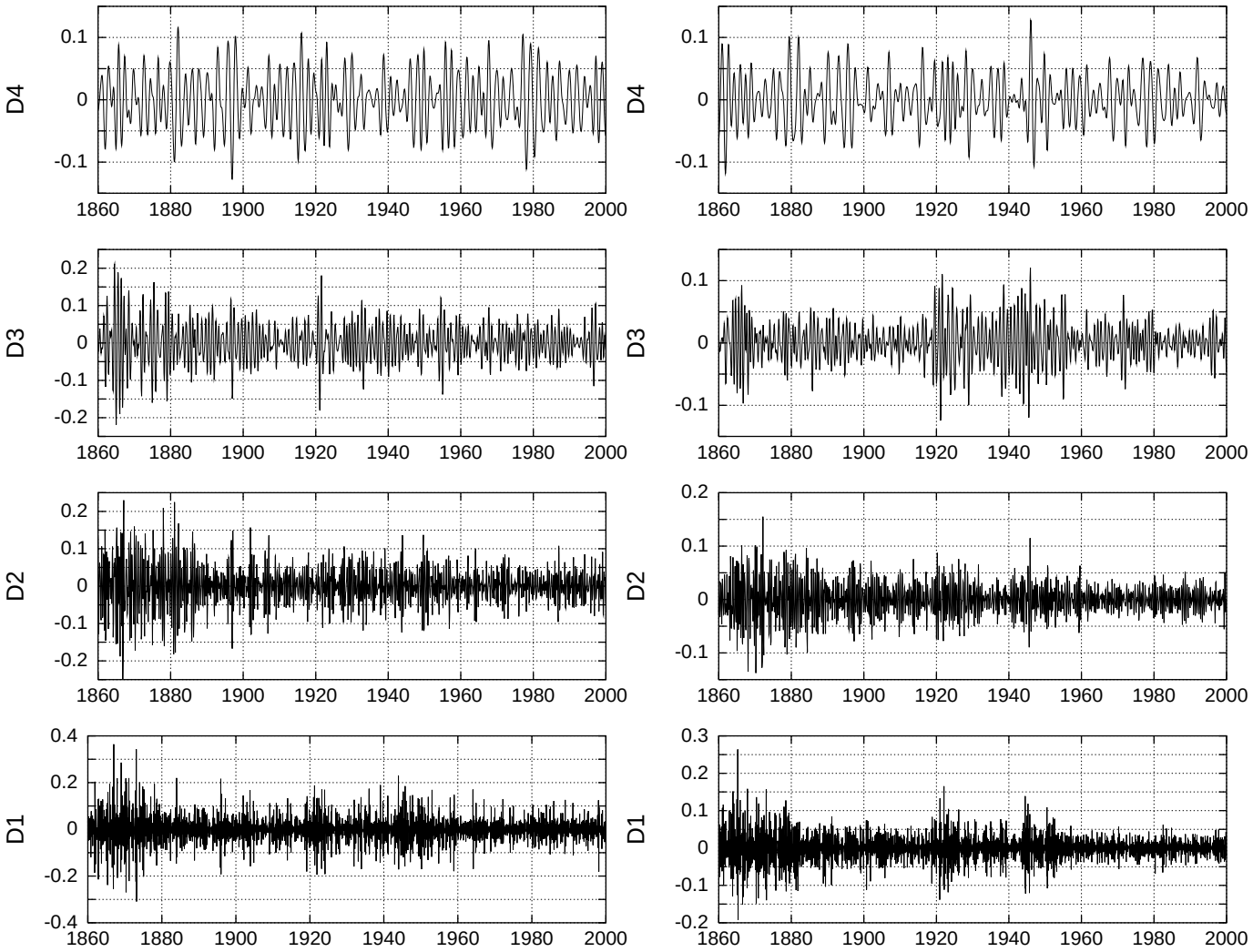

FIG. 4. Wavelet Multiresolution Analysis of the global air (left) and sea (right) temperature anomalies in Celsius degree. The figures show the details D4, D3, D2, D1 that are associated to the scales of 16, 8, 4, 2 months.

Figure 5

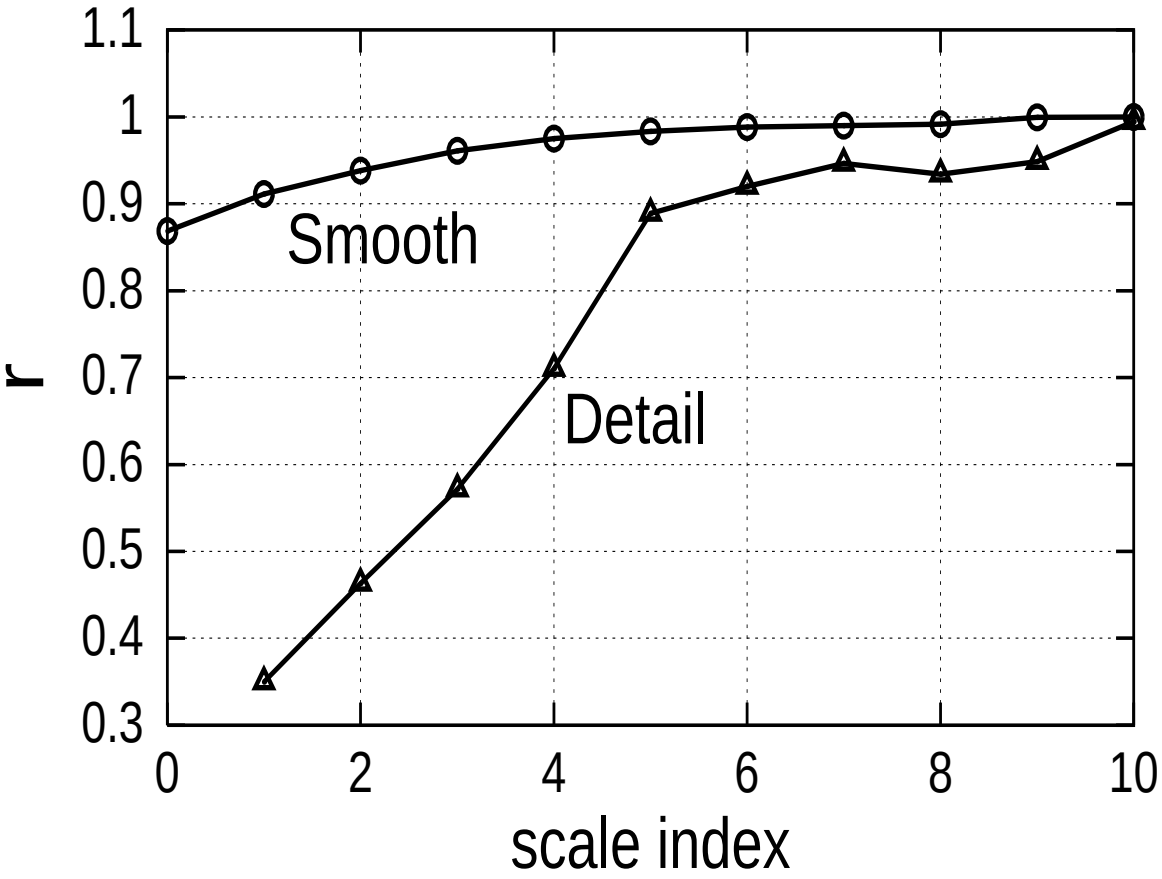

FIG. 5. Correlation coefficient r between the global air and sea temperature anomalies against the wavelet scale index. The top curve denotes the correlation coefficient between the wavelet smooth curves, from S0 to S10. The smooth curves S0 refer to the original data without any filtering. The bottom curve denotes the correlation coefficient between the wavelet detail curves from D1 to D10. See Table II for the value of r.

index	0	1	2	3	4	5	6	7	8	9	10
Smooth	0.87	0.91	0.94	0.96	0.97	0.98	0.99	0.99	0.99	1.00	1.00
Detail		0.35	0.46	0.57	0.71	0.89	0.92	0.95	0.93	0.95	0.99

TABLE II. Correlation coefficient r between the global air and sea temperature anomalies against the wavelet scale index. The value $r = 0.87$ of S0 is the correlation coefficient between the global air and sea temperature anomalies without any filtering.

Figure 6

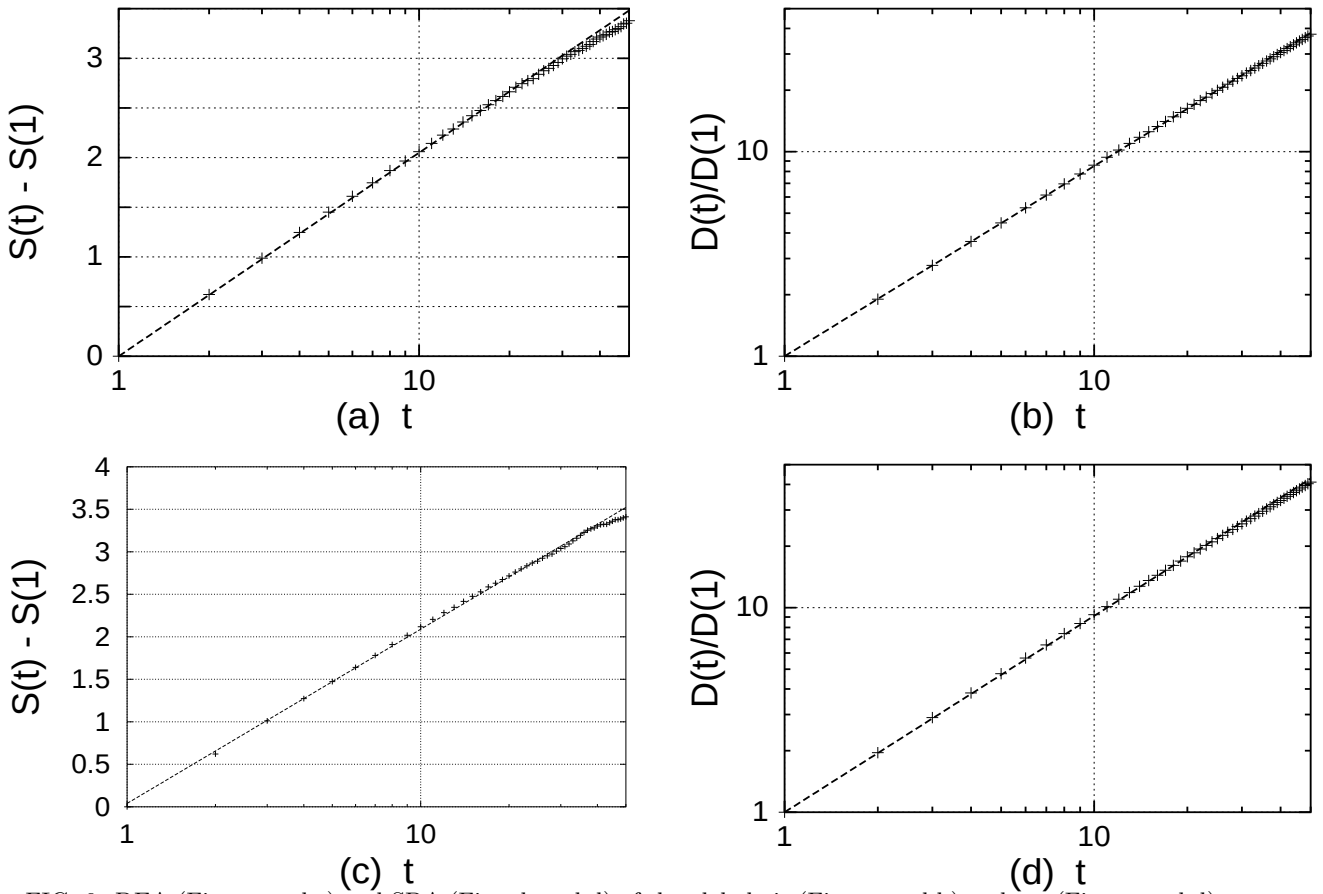

FIG. 6. DEA (Figs. a and c) and SDA (Figs. b and d) of the global air (Figs. a and b) and sea (Figs. c and d) temperature anomalies. The straight lines correspond to functions of the type $f_{DE}(t) = \delta \ \ln(t)$ and $f_{SD}(t) = t^H$, which become straight lines in the linear-log representation of this figure. The global air temperature anomalies are characterized by a pdf scaling coefficient $\delta_a = 0.87 \pm 0.02$ and a standard deviation scaling coefficient $H_a = 0.92 \pm 0.01$. The global sea temperature anomalies are characterized by a pdf scaling coefficient $\delta_s = 0.89 \pm 0.02$ and a standard deviation scaling coefficient $H_s = 0.94 \pm 0.01$.

	H	δ	μ
Air	0.92 ± 0.01	0.87 ± 0.02	2.14 ± 0.02
Sea	0.94 ± 0.01	0.89 ± 0.02	2.12 ± 0.02

TABLE III. Exponents H, δ and μ for the global air and sea temperature anomalies.

Figure 7

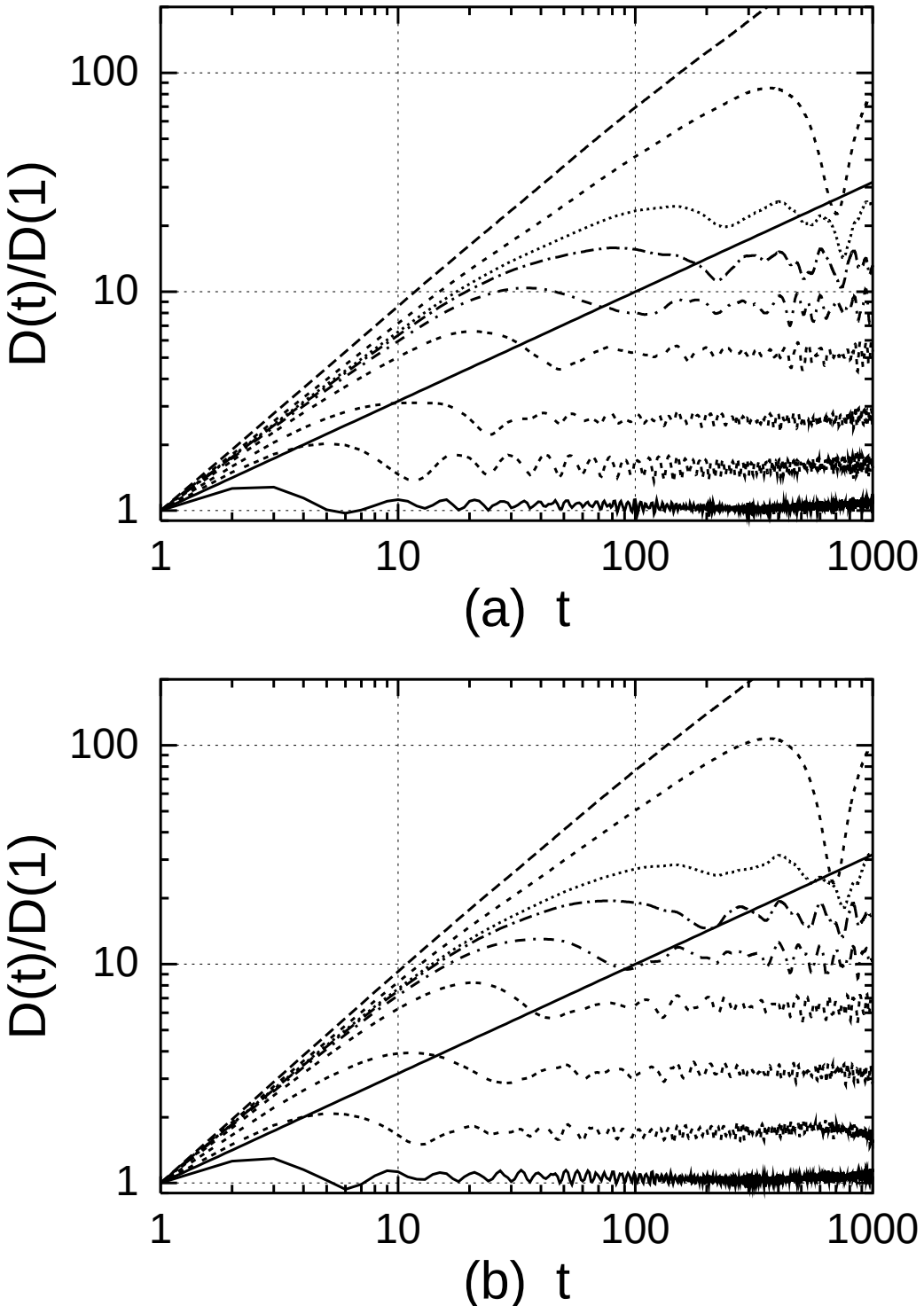

FIG. 7. SDA of the global air (a) and sea (b) temperature anomalies of the residuals R_j. From top to down, the curves are the SDA of (1) the original data, (2) R9, (3) R8,..., (9) R2. The straight line is $f_{SD}(t) = t^{0.5}$ that corresponds to the Gaussian diffusion.

Figure 8

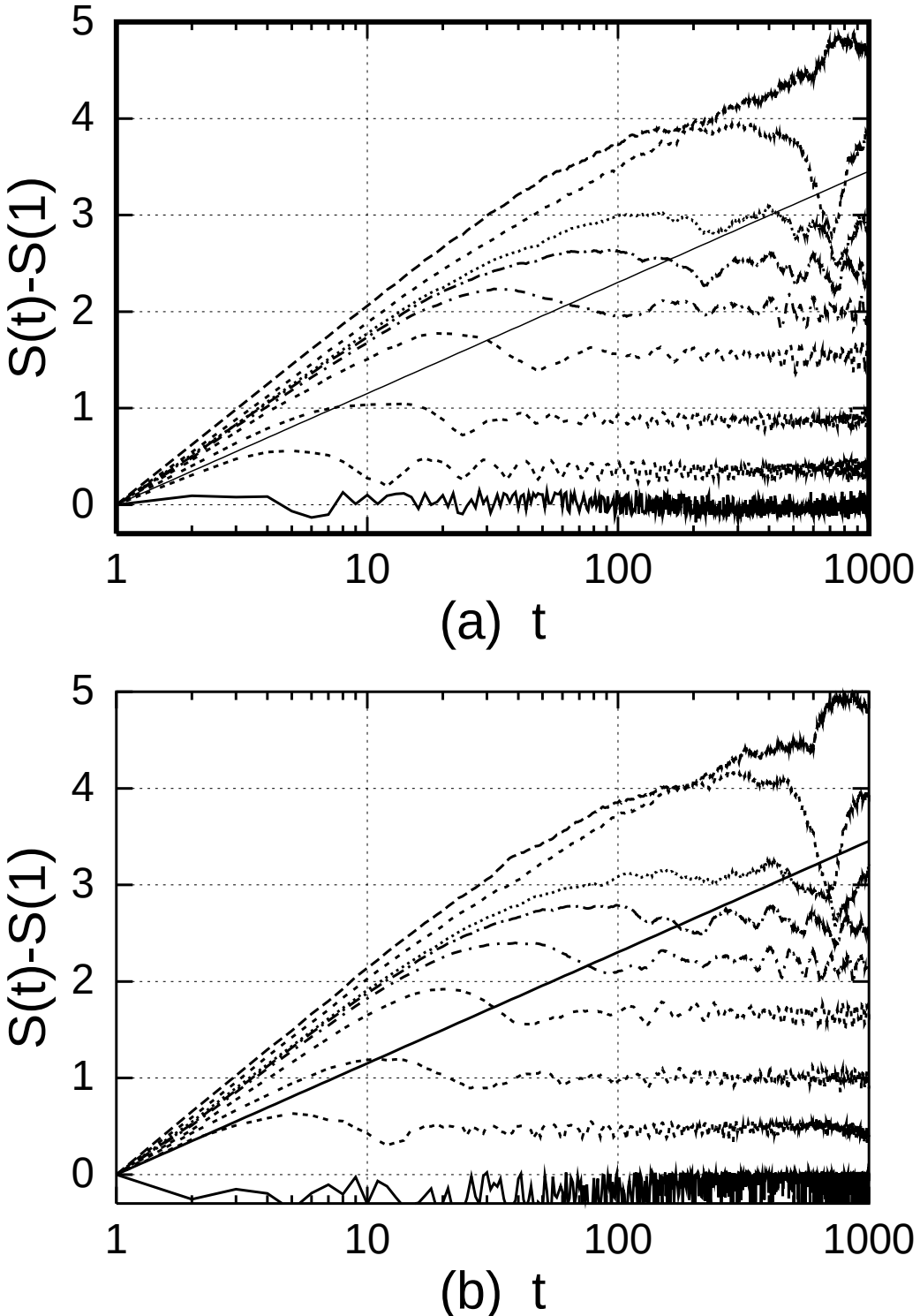

FIG. 8. DEA of the global air (a) and sea (b) temperature anomalies of the residuals R_j. From top to down, the curves are the SDA of (1) the original data, (2) R9, (3) R8,..., (9) R2. The straight line is $f_{DE}(t) = 0.5\ln(t)$ that corresponds to the Gaussian diffusion.

	D(1) Air	D(1) Sea	S(1) Air	S(1) Sea	D_{line} Air	D_{line} Sea	S_{line} Air	S_{line} Sea	D-period Air	S-period Sea
data	0.243	0.221	1.44	1.42						
R9	0.162	0.128	1.09	0.98	23	24	2.80	2.95	707	686
R8	0.158	0.124	1.07	0.96	14	18	2.50	2.60	238	221
R7	0.152	0.117	1.03	0.91	11	14	2.27	2.40	220	211
R6	0.140	0.103	0.96	0.83	7.5	9.5	1.95	2.05	96	93
R5	0.124	0.082	0.85	0.61	4.5	5.7	1.40	1.55	48	48
R4	0.112	0.069	0.82	0.44	2.35	2.90	0.78	0.90	24	24
R3	0.092	0.056	0.69	0.68	1.45	1.55	0.25	0.38	12	12
R2	0.066	0.040	0.43	0.50					6	6

TABLE IV. Summary of the information contained in Figs. 7 and 8. The first four columns report the values of the standard deviation and of the entropy at the first step of diffusion for both global air and sea temperature anomalies and their rests R_j for $j = 2, ..., 9$. The four following columns, from the 5th to the 8th, report the values of the height of the horizontal lines that measures the maximum spreading (in the case of SDA, Figs. 7) and the information or entropy (in the case of DEA, Figs. 8) that corresponds to each wavelet scale. The reported heights are relative to the values of the SDA and DEA at $l = 1$. This means that the SDA and DEA heights are defined by $D_{line} = D_j/D(1)$ and $S_{line} = S_j - S(1)$, respectively, where S_j and D_j are the values of the entropy and of the standard deviation of the diffusion process generated by the residuals R_j. The last two columns report the main periodicities present in each residuals R_j.

Figure 9

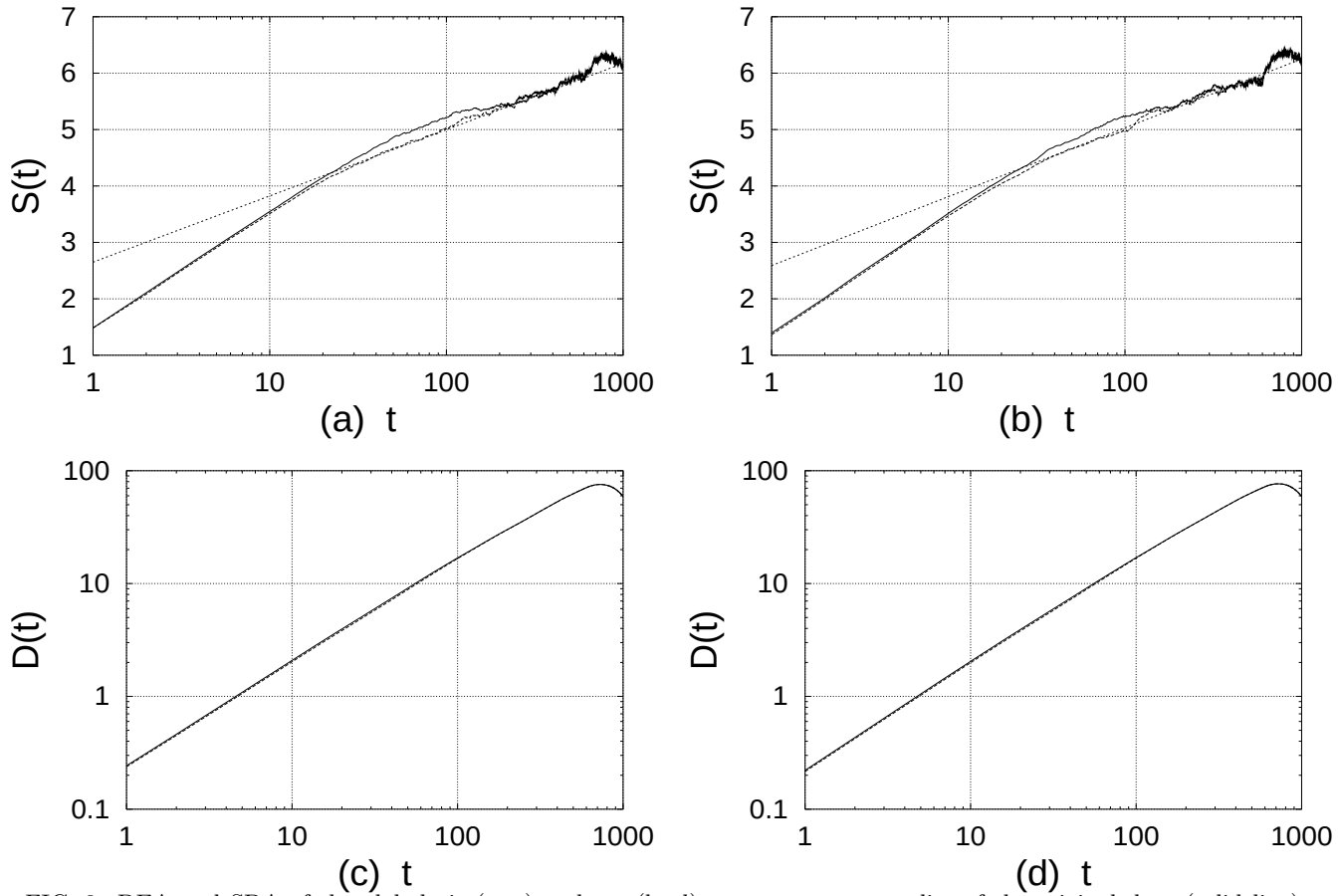

FIG. 9. DEA and SDA of the global air (a, c) and sea (b, d) temperature anomalies of the original data (solid line) and of the data detrended of the detail D7 (dashed line). The straight lines in (a) e (b) have a slope of $\delta = 0.51 \pm 0.02$ (a) and $\delta = 0.53 \pm 0.02$ (b) that correspond to the Gaussian diffusion. The effect of the detail D7 is detected by DEA but not by SDA.